Highly Selective Quantum Sieving of D_2 from H_2 by a Metal−Organic Framework As Determined by Gas Manometry and Infrared Spectroscopy

Stephen A. FitzGerald,*[†] Christopher J. Pierce,[†] Jesse L. C. Rowsell,[‡] Eric D. Bloch,[§] and Jarad A. Mason[§]

[†]Department of Physics and Astronomy, Oberlin College, Oberlin, Ohio 44074, United States
[‡]Department of Chemistry and Biochemistry, Oberlin College, Oberlin, Ohio 44074, United States
[§]Department of Chemistry, University of California, Berkeley, Berkeley, California 94720, United States

S *Supporting Information*

ABSTRACT: The quantum sieving effect between D_2 and H_2 is examined for a series of metal−organic frameworks (MOFs) over the temperature range 77−150 K. Isothermal adsorption measurements demonstrate a consistently larger isosteric heat of adsorption for D_2 vs H_2, with the largest difference being 1.4 kJ/mol in the case of Ni-MOF-74. This leads to a low-pressure selectivity for this material that increases from 1.5 at 150 K to 5.0 at 77 K. Idealized adsorption solution theory indicates that the selectivity decreases with increasing pressure, but remains well above unity at ambient pressure. Infrared measurements

on different MOF materials show a strong correlation between selectivity and the frequency of the adsorbed H_2 translational band. This confirms that the separation is predominantly due to the difference in the zero-point energies of the adsorbed isotopologues.
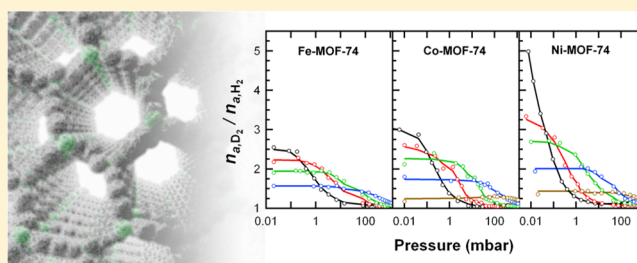
1. INTRODUCTION

Deuterium is a stable isotope that is used extensively in medical and scientific experiments, and as a moderator in heavy water nuclear power stations.[1−3] Its low abundance (0.015 atom % of naturally occurring hydrogen) means that isotopic separation is necessary for all practical applications. Traditionally this has been achieved through the chemical exchange GS (Girdler-sulfide) method in conjunction with cryogenic distillation and electrolysis.[1] However, both the GS and electrolysis steps are highly energy intensive, while the distillation of H_2 (performed at ∼25 K) has a separation factor of only 1.6.[1] Alternate methods have been proposed to overcome these deficiencies, such as isotope exchange,[4] laser isotope separation,[5,6] and gas chromotography,[7] but none have proved practical to date.

Although the isotope effect on physical adsorption has been known for many years, the idea of quantum sieving D_2 from H_2 was first introduced by Beenakker et al.[8] In this scheme, separation is achieved through the difference in the quantum zero-point energy of the adsorbed isotopologues. While the original model used a hard sphere potential in a cylindrical well, subsequent work has performed more realistic simulations of H_2 in confined geometries.[9−11] Using a slit pore model Garberoglio found a selectivity for D_2 over H_2 that decreases from ∼10^4 at 20 K to ∼10 at 100 K in microporous carbons.[12] A similar temperature dependence was calculated for carbon nanotubes, with the selectivity decreasing from 150 at 20 K to 3 at 77 K.[13] Johnson and co-workers used a cylindrical model for carbon nanostructures and predicted selectivities for hydrogen

isotopologues as high as 10^5 (T_2 over H_2) in a (3,6) nanotube at 20 K.[9,14] The authors emphasized the important point that selectivity should increase dramatically as the channel diameter decreases, although it was recently noted that experimental verification of this relationship in single-walled carbon nanotubes is still lacking.[15]

Despite these dramatic predictions there has been little experimental examination of D_2/H_2 separation in adsorbents. In their recent review article Cai et al.[3] pointed out that experimental results show relatively small differences in the adsorption of H_2 and D_2, with selectivities at 77 K typically in the range of 1.0−1.2 for zeolites,[16−18] carbonaceous materials,[19] and metal−organic frameworks (MOFs).[20,21] The largest experimentally determined equilibrium selectivity at 77 K that we are aware of is a value of 1.3 obtained by Noguchi et al. using a MOF known as CuBOTf.[22]

Metal−organic frameworks are a class of materials consisting of metal coordination clusters that are joined together by organic linkers to form microporous structures.[23−26] The crystalline nature of these materials makes them readily amenable to both neutron and X-ray diffraction analyses, and several studies have established the presence of well-defined adsorption sites in archetypal frameworks.[27−31] The primary appeal of these materials is that a myriad of different clusters and organic links can be connected to form, in principle, an

ideal framework with optimal properties for a specific application. Much of the research into MOFs has focused on hydrogen storage and small-molecule separations.[24,25]

One of the most promising MOF structure types is that adopted by the material *catena*-(2,5-dioxidobenzene-1,4-dicarboxylato)dizinc(II), referred to as MOF-74[32] and as Zn-CPO-27.[33] When dehydrated, its pores are lined with exposed metal coordination sites that exhibit some of the highest recorded enthalpies for hydrogen adsorption.[34,35] This framework type is of particular interest because isostructural materials may be prepared with different metal dications (including Mg,[33,36] Mn,[37] Fe,[38] Co,[39] and Ni[32,40]), affording fundamental studies of the metal···H_2 interactions.[41] Studies have shown MOF-74 materials to be highly selective in their adsorption of molecules such as CO_2 over CH_4,[42,43] CO_2 over N_2,[44] and O_2 over N_2.[45] Recently, the Fe analogue was revealed to be highly effective in separating hydrocarbons.[46]

In this report, we evaluate the molecular sieving properties of MOF-74 for the more challenging task of separating D_2 from H_2. We previously used infrared spectroscopy to measure the center-of-mass translational frequencies of adsorbed H_2 at the metal site of the different MOF-74 materials.[41] Some of these frequencies were surprisingly large (in excess of 200 cm^{-1}), indicating a substantial zero-point energy on the order of 400 K. Given the D_2:H_2 mass ratio of 2, one would expect an appreciable difference in their zero-point energies, leading to a large separation factor at low temperature. We observe a strong correlation between the measured infrared frequency and the selectivity of D_2 over H_2 in different MOFs, and inspired by this prospect, we measured H_2 and D_2 adsorption isotherms over a range of temperatures. Supported by idealized adsorption solution theory, our data reveal the highest observed selectivity by quantum sieving at 77 K, a temperature that may be readily employed in separation technology.

2. THEORY

In a solid containing N identical adsorption sites, which may each be occupied by a single adsorbent molecule, the fractional site occupation θ is given by[47]

$$\theta \equiv \frac{n_a}{N} = \frac{z_a(\beta)\, e^{\beta\mu_a}}{1 + z_a(\beta)\, e^{\beta\mu_a}} \tag{1}$$

where n_a is the number of adsorbed molecules, z_a is the canonical partition function of the adsorbed molecule, μ_a is the chemical potential, and β is $(1/k_B T)$ with k_B being Boltzmann's constant and T the absolute temperature. At equilibrium, the chemical potential in the adsorbed phase is equal to that in the gas phase, such that

$$\mu_a = \mu_g = -\frac{1}{\beta} \ln\left(\frac{z_g}{n_g}\right) \tag{2}$$

where n_g is the number of gas molecules, and z_g is the canonical partition function of the ideal gas molecule. This leads to the familiar Langmuir isotherm equation,[48] which assumes that interactions between adsorbed molecules are negligible and that the binding energy at the sites does not change with loading,

$$\theta = \frac{\frac{z_a P V \beta}{z_g}}{1 + \frac{z_a P V \beta}{z_g}} = \frac{P}{P + P^0} \tag{3}$$

where V is volume, P is the gas pressure, and we have defined a characteristic pressure $P_0 \equiv (z_g/z_a)(1/\beta V)$.

In evaluating the partition function we assume that the vibrational, rotational, and translational contributions are separable, such that the partition function of a single molecule is given as

$$z_i = z_i^{\text{vib}} z_i^{\text{rot}} z_i^{\text{trans}} \tag{4}$$

and therefore

$$\frac{z_g}{z_a} = \frac{z_g^{\text{vib}}}{z_a^{\text{vib}}} \frac{z_g^{\text{rot}}}{z_a^{\text{rot}}} \frac{z_g^{\text{trans}}}{z_a^{\text{trans}}} \tag{5}$$

The vibrational frequency of H_2 is sufficiently large that even at room temperature virtually all of the molecules are in the ground state, and thus $(z_a^{\text{vib}}/z_g^{\text{vib}}) \approx 1$. The translational partition function ratio is expected to produce the largest deviation from unity. Assuming ideal gas behavior[47]

$$z_g^{\text{trans}} = V\left(\frac{m}{2\pi\beta\hbar^2}\right)^{3/2} \tag{6}$$

where m is the molecular mass. For z_a, we extend the approach of Trasca et al. to a three-dimensional confining potential,[10] and treat the molecule as a point mass moving within an isotropic, simple harmonic potential well with energy levels $\varepsilon_{n_x,n_y,n_z} = (n_x + n_y + n_z + 3/2)\,\hbar\omega$, where n_x, n_y, and n_z are the respective quantum numbers and ω is the translational angular frequency. We define the classical binding energy, ε_c, as the energy at the bottom of the potential well, such that in the 3-d simple harmonic approximation, the true binding energy is given by $\varepsilon_b = \varepsilon_c + (3/2)\,\hbar\omega$ (these definitions are illustrated in Figure S1 of the Supporting Information [SI]). This leads to

$$z_a^{\text{trans}} = e^{-\varepsilon_c}\left[\sum_{n=0}^{\infty} e^{-\beta\hbar\omega\left(n+\frac{1}{2}\right)}\right]^3 = \frac{e^{-\beta\varepsilon_b}}{(1 - e^{-\hbar\omega\beta})^3} \tag{7}$$

Combining this with the expression for the translational partition function of the ideal gas, we complete our definition of the characteristic pressure P^0 in the Langmuir isotherm.

$$P^0 = \beta^{-5/2}\left(\frac{m}{2\pi\hbar^2}\right)^{3/2} (1 - e^{-\beta\hbar\omega})^3\, e^{\beta\varepsilon_b}\frac{z_g^{\text{rot}}}{z_a^{\text{rot}}} \tag{8}$$

The next step is to extend the model to describe adsorption in materials with multiple distinct sites. If we again assume that interactions between adsorbed molecules on neighboring sites can be neglected, then the total number of sites occupied is just the sum over Langmuir isotherms for the different types of site:

$$n_a = \sum_i \frac{N_i P}{P + P_i^0} \tag{9}$$

where N_i is the number of available sites with characteristic pressure P_i^0

3. EXPERIMENTAL PROCEDURE

The synthesis and characterization of the MOF samples used in this paper have been presented in our previous reports.[41,49] The infrared measurements of the adsorbed molecular hydrogen were performed using the diffuse reflectance technique outlined in our earlier work.[50] This technique significantly enhances the IR signal of adsorbed hydrogen in comparison to more traditional transmission measurements. A custom-built cryogenic chamber allows the sample powders

to be mounted, degassed, cooled, and dosed with hydrogen without exposing them to air.[51]

Gas adsorption isotherms were measured using a Micromeritics ASAP 2020 instrument. Dosing calculations were performed using the real gas equations of state for both H_2 and D_2 in conjunction with thermal transpiration corrections.[52] Free space determination was performed using high purity He gas. The MOF samples were transferred within an argon glovebox to the sealed measurement vessel preventing any air exposure. Measurements were performed using both a standard Micromeritics glass sample tube and a custom-built copper cell that was mounted on a Janis closed-cycle helium refrigerator. The sample temperature was determined using a Si-diode thermometer mounted on the sample cell. The reliability of the thermometer to accurately reflect the sample temperature was confirmed via control adsorption isotherms with the copper cell immersed in liquid nitrogen.

4. RESULTS AND DISCUSSION

4.1. Isotherms. Measuring the quantity of a particular gas adsorbed as a function of loading pressure for a given temperature (an adsorption isotherm) is a standard way to characterize a material's adsorptive behavior. Figure 1 shows a
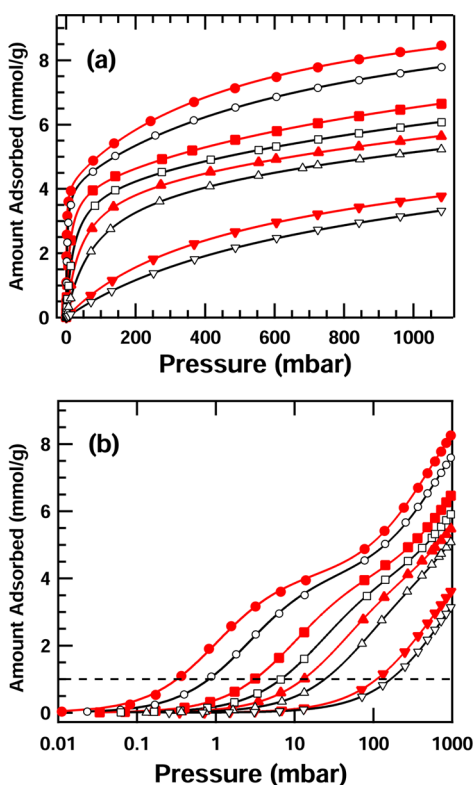

Figure 1. (a) D_2 (red, filled symbols) and H_2 (black, open symbols) adsorption isotherms for Fe-MOF-74 at 77 K (○), 90 K (□), 100 K (△), and 120 K (▽). Curves are fits to the constrained two-site Langmuir model. (b) Data are replotted on a logarithmic scale to emphasize the fit at low pressure. The dashed line is illustrative for determining Q_{st} (see description in text).

series of such H_2 and D_2 adsorption isotherms obtained from Fe-MOF-74. At all temperatures we see the adsorption of D_2 is consistently larger than that of H_2. The H_2 adsorption isotherm at 77 K is similar to that obtained previously,[53] showing a steep initial rise followed by a gradual increase at higher pressure. The initial loading is attributed to H_2 binding at the metal site and was confirmed by neutron diffraction experiments.[53] These

neutron diffraction results are consistent with earlier studies of the Mg and Zn analogues.[31,54] Queen et al. successfully modeled their Fe-MOF-74 adsorption isotherms at 77 and 87 K using a two-site Langmuir model.[53] We now extend this approach to higher temperature and show that the model works equally well for D_2. As shown in Figure 1 the agreement between data and fit is excellent, with Figure 1b (presented on a logarithmic scale) emphasizing the agreement at low pressure. The site saturation numbers, N_1 and N_2, are constrained to be the same for all eight isotherms and the only parameters that are free to change with isotopologue and temperature are P_1^0 and P_2^0. These values are presented in Table 1. Consistent with

Table 1. Two-Site Langmuir Model Fit Parameters for H_2 and D_2 in Fe-MOF-74[a]

T (K)	P_{1,H_2}^0	P_{1,D_2}^0	P_{2,H_2}^0	P_{2,D_2}^0
77	2.56	1.00	800	538
90	21.4	9.8	2300	1610
100	79.5	41.6	3850	3030
120	604	384	9030	8230

[a]N_1 = 4.1 mmol/g and N_2 = 6.4 mmol/g are the saturation loadings for the primary and secondary sites, respectively, obtained from the model and applied to all isotherms. Pressures are in mbar.

the predictions of eq 8, the P^0 values increase in a highly nonlinear fashion with increasing temperature and as expected the enhanced adsorption of D_2 over H_2 is manifest through D_2 having consistently lower P^0 values.

4.2. Isosteric Heat. This enhanced adsorption can be quantified in terms of the often-used isosteric heat of adsorption,

$$Q_{st} = RT^2 \left[\frac{\partial \ln P}{\partial T} \right]_{n_a} = -\left[\frac{\partial \ln P}{\partial \beta} \right]_{n_a} \quad (10)$$

where n_a is a fixed quantity in the partial derivative. The isosteric heat is generally calculated from isothermal measurements obtained at two or more temperatures. For example, as shown in Figure 1, the dashed line at 1 mmol/g could be used to determine the temperature dependent P values for this particular n_a loading. However, the experimental data points obtained at different temperatures typically do not have precisely the same loading and so some form of interpolation is required. There are different schemes for doing this, and as recently shown in the case of Fe-MOF-74 which has a very sharp inflection point, even subtle variations in the interpolation can lead to large variations in the calculated Q_{st} curve.[53] This is especially true at low n_a values where errors in the pressure measurements of the individual points are greatly magnified.

The advantage of the two-site Langmuir model used to fit the data in Figure 1 is that the expression can be inverted via a simple quadratic equation to obtain P as a function of n_a.[55] This can then be used to generate a continuous Q_{st} curve as a function of n_a. The P^0 values used to generate this curve are determined from fits of all the isotherm data and are, therefore, less affected by sensitivity limitations at low pressure. Additionally, it allows Q_{st} values to be more confidently extrapolated to both a zero and a high loading Q_{st} limit. Figure 2 shows the Q_{st} curves obtained in this way for H_2 and D_2 in Fe, Co, and Ni-MOF-74. (The isotherm data for Co and Ni and corresponding two-site Langmuir model fit parameters are
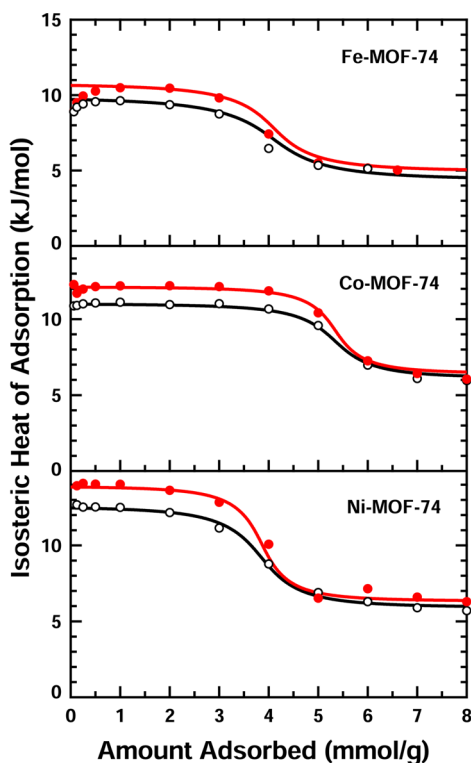
Figure 2. Isosteric heat of adsorption for both D_2 (red, filled circles) and H_2 (black, open circles) as a function of coverage for Ni, Fe, and Co-MOF-74. The curves are generated using the constrained two-site Langmuir model and the symbols are the result of numerical interpolation of the respective adsorption isotherms using a virial expansion.

included in the SI Figures S2 and S3 and Tables S1 and S2). The overall values are consistent with previous theoretical estimates.[37,56] Included as points are the values obtained from the more standard numerical approach in which the isotherms are modeled using a virial expansion.[57] In all cases the Q_{st} curves show a sharp decrease in value between 4 and 5 mmol/g. This reflects the filling of the metal site followed by subsequent loading at the less attractive "oxygen site".[31] In principle, the drop in Q_{st} would be infinitely sharp at zero Kelvin and become more smeared out at higher temperature where occupancy of the secondary (oxygen) site occurs before saturation of the primary (metal) site.

In all three cases the Q_{st} for D_2 is significantly higher at the primary (metal site) than that of H_2. The difference in Q_{st} extrapolated to zero coverage increases from 0.9 kJ/mol for Fe, to 1.1 kJ/mol for Co, to 1.4 kJ/mol for Ni. As expected, this difference is much smaller at higher concentration where the primary site is saturated and adsorption occurs at the secondary sites.

The enhanced Q_{st} for D_2 can be explained in terms of the reduced translational zero-point energy experienced by D_2 at a particular binding site. Focusing on the initial loading that occurs in the low pressure limit, we note that (as shown in Table 1) the P_1^0 values are at least an order of magnitude less than the equivalent P_2^0 values. Thus, to a good approximation the initial adsorption is dominated by the metal site, and we need only consider a single-site Langmuir model in the low pressure limit. Combining eqs 3, 8, and 10 yields

$$Q_{st} = -\varepsilon_b + \frac{5}{2}k_B T - \frac{3\hbar\omega\ e^{-\beta\hbar\omega}}{1 - e^{-\beta\hbar\omega}} + \frac{\partial}{\partial\beta}\left[\ln\left(\frac{z_a^{rot}}{z_g^{rot}}\right)\right]$$

(11)

Neglecting the rotational terms, we see that the limit of $Q_{st} \approx -\varepsilon_b$ as $T \to 0$ K. The difference in ε_b between D_2 and H_2 is given by

$$-\Delta\varepsilon_b = \varepsilon_{b,H_2} - \varepsilon_{b,D_2}$$
$$= (3/2)\hbar(\omega_{H_2} - \omega_{D_2})$$
$$= (3/2)\hbar\omega_{H_2}(1 - 1/\sqrt{2})$$

(12)

where we have assumed that H_2 and D_2 behave chemically identically and that within the harmonic approximation $\omega_{D_2} \approx (\omega_{H_2}/\sqrt{2})$. In our earlier infrared work on adsorbed H_2 (and shown in Figure S5 of the SI) we measured the center-of-mass translational frequencies for H_2 in Ni, Co, and Fe-MOF-74 to be 212, 185, and 147 cm^{-1} respectively.[41] Using these values, eq 12 yields $-\Delta\varepsilon_b$ values of 1.11, 0.97, and 0.77 kJ/mol. These are similar to, but less than, our measured ΔQ_{st} values of 1.4, 1.1, and 0.9 kJ/mol. It thus appears that the majority of the difference in the behavior between H_2 and D_2 can be attributed to the difference in their translational zero-point energy.

As shown by the last two columns in Table 2, the theoretical differences in Q_{st} between D_2 and H_2, $\Delta(Q_{st}^{th})$, are reduced

Table 2. Zero-Loading Q_{st} Values for Ni, Co, and Fe-MOF-74 As Determined from Isotherm Measurements with H_2 and D_2[a]

metal	Q_{st,H_2}	Q_{st,D_2}	ΔQ_{st}	$-\Delta\varepsilon_b$	ΔQ_{st}^{th}
Ni	12.5	13.8	1.4	1.11	0.92
Co	11.0	12.1	1.1	0.97	0.74
Fe	9.7	10.6	0.9	0.77	0.51

[a]As per eq 12, $-\Delta\varepsilon_b$ is the difference in translational zero-point energy determined from infrared spectra and assuming a 3-d simple harmonic oscillator potential. ΔQ_{st}^{th} is the theoretical value at 77 K based on eq 11 and neglecting rotational contributions. All energies are in kJ/mol.

when finite temperature terms are included. The discrepancies between our theoretical and experimental values are most likely due to anharmonic contributions to the translational motion, and the fact that we have not factored in the rotational term. Both inelastic neutron scattering[53,54,58] and infrared spectroscopy[41,49] show that the H_2 rotational levels are significantly perturbed from their gas phase values when adsorbed in MOF-74. For practical reasons, neither technique has been able to generate spectra for the rotational levels of adsorbed D_2.

Computational models of H_2/D_2 in carbon nanotubes have shown that, when the channel dimensions are comparable to the molecular kinetic diameter, adsorbate rotation is strongly hindered and the rotational zero-point energy becomes sufficiently large to hamper the adsorption of H_2 relative to that of D_2.[15] This confinement effect is expected to be much less important for the MOF-74 structure type, where the channel diameter is 1.1 nm, after accounting for the van der Waals radii of the framework atoms. We note that Kong et al. estimated the rotational zero-point energy for H_2 in Zn-MOF-74 to be on the order of 1 kJ/mol and less than 10% of the binding energy.[56]

Modeling the rotational contribution to ΔQ_{st} is challenging because the main contribution appears to be due to rotational–translational coupling.[10,59] The orientational interactions between H_2 and the MOF must be averaged over the zero-point motion (translational ground state) of the adsorbed molecule. Quantum mechanically, the heavier mass of D_2 leads to a narrower translational wave function, and it is expected to act as a smaller molecule. Thus, a complete calculation would require a coupled five-dimensional potential energy analysis. Due to the complexity of the MOF-74 structure, this coupling was excluded in previous theoretical studies,[37,56] and such an analysis is beyond the scope of this paper.

4.3. Selectivity. The simplest way to quantify the preferential adsorption of D_2 over H_2 is to divide the adsorbed quantity of D_2 by that of H_2 at the same pressure. This information is presented in Figure S4 of the SI. Overall, the magnitude of the enhancement is quite dramatic, reaching a value close to 5 for Ni-MOF-74 at 77 K. This is in comparison with the highest previously recorded equilibrium value for adsorption selectivity at 77 K of 1.3.[22] While the data presented in this way offer a simple experimental quantification of the enhanced adsorption of D_2 over H_2, they do not express the actual selectivity that would be obtained with a gas mixture. The selectivity is defined as the ratio of molar fractions in the adsorbed phase (x) and gas phase (y),[9]

$$S = \frac{x_{D_2}/y_{D_2}}{x_{H_2}/y_{H_2}} = \frac{n_{a,D_2}/n_{g,D_2}}{n_{a,H_2}/n_{g,H_2}} \tag{13}$$

and can only be measured directly through experiments with gas mixtures. This requires a technique that can discriminate between adsorbed D_2 and H_2 when mixed. In the absence of such a technique it is possible to derive a selectivity from single-component adsorption isotherms using idealized adsorption solution theory (IAST).[60] This theory assumes that (i) the same surface area is available to both adsorptives, (ii) the adsorbent is inert, and (iii) the mixture behaves as an ideal solution described by Raoult's law. Previous studies applied this theory to hydrogen isotopologue mixtures[22,61] and in a recent report Cessford et al.[62] demonstrated the applicability of IAST to adsorption in MOFs.

Within the two-site Langmuir model the IAST selectivity is obtained by solving an equation of the form[61]

$$\sum_{i=1}^{2} N_i \left[\ln\left(1 + \frac{P}{P_{i,H_2}^0} \frac{y_{H_2}}{x_{H_2}}\right) - \ln\left(1 + \frac{P}{P_{i,D_2}^0} \frac{y_{D_2}}{x_{D_2}}\right) \right] = 0 \tag{14}$$

combined with the fact that $x_{D_2} = 1 - x_{H_2}$. In the zero-pressure limit the selectivity reduces to

$$S_0 = \frac{P_{1,H_2}^0}{P_{1,D_2}^0} \tag{15}$$

Figure 3 shows the selectivity determined (for a 50/50 gas mixture, i.e. $y_{D_2} = y_{H_2} = 1/2$) by an IAST analysis of the experimental isotherms with Fe, Co, and Ni-MOF-74. In all cases the values are well above unity and as predicted by eq 15 the selectivity converges to the simple ratio of the two isotherms (illustrated by the dashed lines) in the zero-pressure limit. In the case of Ni-MOF-74 there is a slight discrepancy, reflecting the fact that for Ni the two-site Langmuir model is
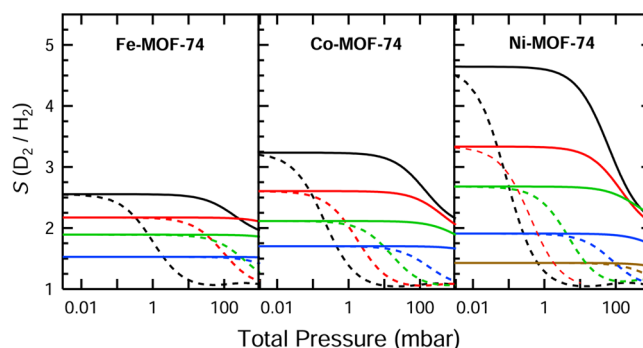

Figure 3. Selectivity (solid curves) of D_2 over H_2 as determined by an IAST analysis of the experimental isotherms at 77 K (black), 87 K (red), 100 K (green), 120 K (blue), and 150 K (brown). The dashed curves show the $n_{a,D_2}/n_{a,H_2}$ ratio at the same temperatures as determined by the two-site Langmuir fit.

not as good a fit as the other materials. This large selectivity is maintained to higher pressure than suggested by the pure-component isotherm ratio and reflects the fact that in a mixture there is direct competition for the metal site. Even at a partial pressure where H_2 would fully occupy the site, D_2 is capable of displacing it, leading to the observed high selectivity. This result extends the useful pressure range of a material and thus the feasibility of using these MOFs in a practical separation system. In the case of Ni-MOF-74 the 77 K selectivity exceeds 2 at a pressure of 1 atm.

As stated above, the zero-pressure selectivity reduces to the simple ratio of the respective isotherms and thus its value can be determined directly by measuring the initial slopes of the adsorption isotherms within the low-pressure (Henry's law) limit. Figure 4 shows the experimentally observed temperature dependence of this zero-pressure limit selectivity for the different MOF-74 materials. In each case the selectivity increases in a nonlinear fashion with decreasing temperature, with the Ni sample displaying by far the largest increase. On the basis of eq 16 (see below) the temperature dependence is
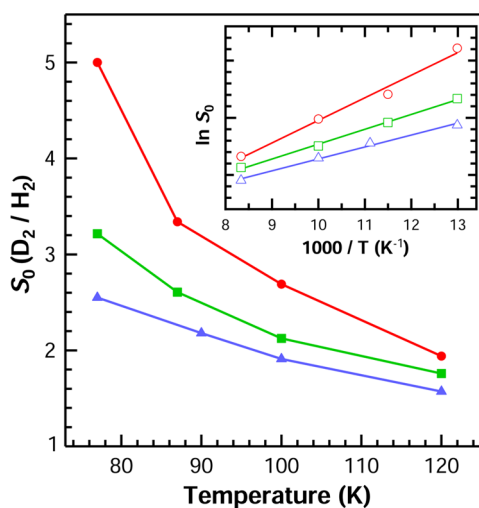

Figure 4. Zero-pressure-limit selectivity as a function of temperature for Ni (red circles), Co (green squares), and Fe (blue triangles) MOF-74. Data are based on the initial slope of the adsorption isotherms for pressures at least an order of magnitude less than the corresponding P_1^0 value. The inset shows the same data as an Arrhenius law plot.

determined by the product of an exponential term times a ratio term which is estimated to vary by no more than 20% over the range in question. The inset in Figure 4 shows the selectivity as an Arrhenius law plot. This confirms that the behavior is dominated by the exponential term and that this approach can be used to estimate the selectivity at lower temperature. Extrapolation of the Arrhenius plot to 25 K, the temperature used in H_2/D_2 distillation,[1] indicates a selectivity on the order of 1000 for the Ni material. This selectivity comes with the price that it can only be achieved at very low pressures below P_2^0 which is similarly estimated to be on the order of 10^{-10} bar at 25 K. Above this pressure the secondary site is significantly populated and IAST shows the selectivity decreasing to a value on the order of 100. Within our simple two-site model this level of selectivity is maintained at all higher pressures, however in practice the occupancy of tertiary and quaternary sites should lead to further decreases in the selectivity.

4.4. Translational Mode Frequency. As outlined in the Theory section, the principle factor producing these large selectivities is expected to be the excess translational zero-point energy of H_2 over D_2. To further understand this behavior, we can combine the 3-d simple harmonic energy definition with eqs 8 and 15 to yield

$$S_0 = \left(\frac{m_{H_2}}{m_{D_2}}\right)^{3/2}\left(\frac{1 - e^{-\beta\hbar\omega_{H_2}}}{1 - e^{-\beta\hbar\omega_{D_2}}}\right)^3 e^{\frac{3}{2}\beta\hbar(\omega_{H_2}-\omega_{D_2})}\left(\frac{z_{g,H_2}^{rot}}{z_{a,H_2}^{rot}}\right)\left(\frac{z_{a,D_2}^{rot}}{z_{g,D_2}^{rot}}\right)$$

(16)

The selectivity depends critically on the difference in frequency between H_2 and D_2, and if we again assume that $\omega_{D_2} \approx (\omega_{H_2}/\sqrt{2})$ then the selectivity should increase nearly exponentially with the H_2 translational frequency.

Figure 5 shows the 77 K zero-pressure limit selectivity for different MOF materials as a function of the experimentally
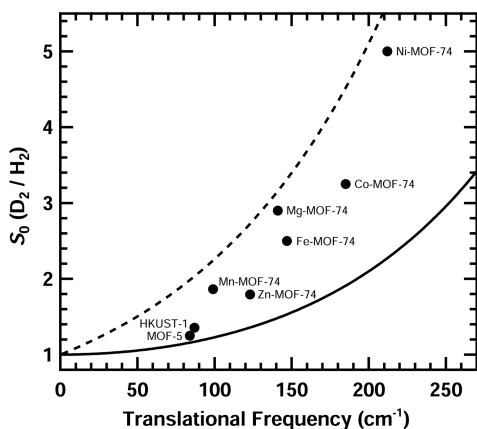

Figure 5. Zero-pressure selectivity at 77 K for MOF materials as a function of the infrared translational mode frequency. The solid line shows the prediction based on eq 16, while the dashed line indicates the Boltzmann factor contribution arising from the difference in the translation zero-point energy between H_2 and D_2.

measured translational mode frequency of the adsorbed H_2 (see Figure S5 in SI). Plotted in this way, we see that there is indeed a dramatic increase in selectivity with frequency. In addition to the three previously discussed materials we also measured Mn, Mg, and Zn-MOF-74 along with two archetypal MOFs known as MOF-5 and HKUST-1.[63,64] In the case of the standard MOF-5 and HKUST-1 we see that their low translational

frequencies correlate with typical small selectivities (i.e. less than 1.3) observed by other groups.[20−22] In contrast, the higher translational frequencies of adsorbed H_2 in the MOF-74 materials yield much larger selectivities. This provides clear evidence that the dominant indicator of an adsorbent's performance in separating D_2 and H_2 is the translational frequency of the bound molecule. In our opinion, the spectroscopic analysis we have described here is an experimentally practical method for evaluating candidate materials.

The dashed curve in Figure 5 shows the predicted selectivity arising solely from the Boltzmann factor difference in the translational zero-point energy (within the harmonic approximation). The solid curve shows the full translational contribution to the selectivity based on eq 16. The experimental values lie between these two curves. As with the Q_{st} comparison, we expect both rotational and anharmonic terms to modify the final selectivity curve. Since the selectivity depends exponentially on the zero-point energy difference, we would expect it to be far more sensitive to the limitations of our model.

Finally, we note that all the experimental data presented in this paper are equilibrium-based measurements that do not reflect possible effects due to differences in the kinetic behavior of H_2 and D_2. Recently, Niimura et al. investigated these effects in zeolite and carbon-based materials.[65] Their 77 K data indicate a dynamic selectivity of 3.05 in MS13X zeolite. We have also observed kinetic differences in the behavior of H_2 and D_2 within MOF-74 and are in the process of exploring them further.

5. SUMMARY

For MOF-74 materials, adsorption isotherms indicate a significantly larger initial isosteric heat of adsorption for D_2 over H_2. This increase is primarily attributed to the difference in the zero-point energies of the isotopologues when they are adsorbed at the metal site. This behavior leads to some of the highest reported D_2/H_2 selectivities in microporous adsorbents, up to 5 at 77 K. In the case of Ni-MOF-74 the 77 K enrichment factor is more than three times greater than that employed in the distillation process. Infrared measurements on a number of different MOF materials reveal a strong correlation between selectivity and the translational mode frequency of the adsorbed molecule. This should prove central to the optimization of future porous materials for D_2 separation.

■ ASSOCIATED CONTENT

ⓢ Supporting Information

Illustrative energy scheme for adsorbed H_2, additional isotherms and fitting parameters, ratio of isotherms for D_2 to H_2, and infrared spectra for a range of MOF materials showing the center-of-mass translational mode. This material is available free of charge via the Internet at http://pubs.acs.org.

■ AUTHOR INFORMATION

Corresponding Author
stephen.fitzgerald@oberlin.edu

Notes
The authors declare no competing financial interest.

REFERENCES

(1) Rae, H. K. *Selecting Heavy Water Processes*; ACS Symposium Series *68*, American Chemical Society: Washington, DC1978.

(2) Chu, X. Z.; Zhao, Y. J.; Kan, Y. H.; Zhang, W. G.; Zhou, S. Y.; Zhou, Y. P.; Zhou, L. *Chem. Eng. J.* **2009**, *152*, 428.

(3) Cai, J. J.; Xing, Y. L.; Zhao, X. B. *RSC Adv.* **2012**, *2*, 8579.

(4) Luo, W. F.; Cowgill, D. F.; Causey, R. A. *J. Phys. Chem. B* **2009**, *113*, 12978.

(5) Atabek, O.; Chrysos, M.; Lefebvre, R. *Phys. Rev. A* **1994**, *49*, R8.

(6) Averbukh, I. S.; Vrakking, M. J. J.; Villeneuve, D. M.; Stolow, A. *Phys. Rev. Lett.* **1996**, *77*, 3518.

(7) Fukada, S.; Fujiwara, H. *J. Chromatogr. A* **2000**, *898*, 125.

(8) Beenakker, J. J. M.; Borman, V. D.; Krylov, S. Y. *Chem. Phys. Lett.* **1995**, *232*, 379.

(9) Wang, Q. Y.; Challa, S. R.; Sholl, D. S.; Johnson, J. K. *Phys. Rev. Lett.* **1999**, *82*, 956.

(10) Trasca, R. A.; Kostov, M. K.; Cole, M. W. *Phys. Rev. B* **2003**, *67*, 35410.

(11) Kumar, A. V. A.; Bhatia, S. K. *Phys. Rev. Lett.* **2005**, *95*, 245901.

(12) Garberoglio, G. *Eur. Phys. J. D* **2009**, *51*, 185.

(13) Garberoglio, G. *J. Chem. Phys.* **2008**, *128*, 134109.

(14) Challa, S. R.; Sholl, D. S.; Johnson, J. K. *Phys. Rev. B* **2001**, *63*, 245419.

(15) Garberoglio, G.; Johnson, J. K. *ACS Nano* **2010**, *4*, 1703.

(16) Stephanie-Victoire, F.; Goulay, A. M.; de Lara, E. C. *Langmuir* **1998**, *14*, 7255.

(17) Kotoh, K.; Nishikawa, T.; Kashio, Y. *J. Nucl. Sci. Technol.* **2002**, *39*, 435.

(18) Chu, X.-Z.; Zhou, Y.-P.; Zhang, Y.-Z.; Su, W.; Sun, Y.; Zhou, L. *J. Phys. Chem. B* **2006**, *110*, 22596.

(19) Zhao, X. B.; Villar-Rodil, S.; Fletcher, A. J.; Thomas, K. M. *J. Phys. Chem. B* **2006**, *110*, 9947.

(20) Xiao, B.; Wheatley, P. S.; Zhao, X. B.; Fletcher, A. J.; Fox, S.; Rossi, A. G.; Megson, I. L.; Bordiga, S.; Regli, L.; Thomas, K. M.; Morris, R. E. *J. Am. Chem. Soc.* **2007**, *129*, 1203.

(21) Chen, B.; Zhao, X.; Putkham, A.; Hong, K.; Lobkovsky, E. B.; Hurtado, E. J.; Fletcher, A. J.; Thomas, K. M. *J. Am. Chem. Soc.* **2008**, *130*, 6411.

(22) Noguchi, D.; Tanaka, H.; Kondo, A.; Kajiro, H.; Noguchi, H.; Ohba, T.; Kanoh, H.; Kaneko, K. *J. Am. Chem. Soc.* **2008**, *130*, 6367.

(23) Rowsell, J. L. C.; Yaghi, O. M. *Microporous Mesoporous Mat.* **2004**, *73*, 3.

(24) Dincă, M.; Long, J. R. *Angew. Chem. Int. Ed.* **2008**, *47*, 6766.

(25) Li, J. R.; Kuppler, R. J.; Zhou, H. C. *Chem. Soc. Rev.* **2009**, *38*, 1477.

(26) Murray, L. J.; Dincă, M.; Long, J. R. *Chem. Soc. Rev.* **2009**, *38*, 1294.

(27) Rowsell, J. L. C.; Spencer, E. C.; Eckert, J.; Howard, J. A. K.; Yaghi, O. M. *Science* **2005**, *309*, 1350.

(28) Yildirim, T.; Hartman, M. R. *Phys. Rev. Lett.* **2005**, *95*, 215504.

(29) Spencer, E. C.; Howard, J. A. K.; McIntyre, G. J.; Rowsell, J. L. C.; Yaghi, O. M. *Chem. Commun.* **2006**, *3*, 278.

(30) Peterson, V. K.; Liu, Y.; Brown, C. M.; Kepert, C. J. *J. Am. Chem. Soc.* **2006**, *128*, 15578.

(31) Liu, Y.; Kabbour, H.; Brown, C. M.; Neumann, D. A.; Ahn, C. C. *Langmuir* **2008**, *24*, 4772.

(32) Rosi, N. L.; Kim, J.; Eddaoudi, M.; Chen, B. L.; O'Keeffe, M.; Yaghi, O. M. *J. Am. Chem. Soc.* **2005**, *127*, 1504.

(33) Dietzel, P. D. C.; Johnsen, R. E.; Blom, R.; Fjellvåg, H. *Chem.— Eur. J.* **2008**, *14*, 2389.

(34) Rowsell, J. L. C.; Yaghi, O. M. *J. Am. Chem. Soc.* **2006**, *128*, 1304.

(35) Vitillo, J. G.; Regli, L.; Chavan, S.; Ricchiardi, G.; Spoto, G.; Dietzel, P. D. C.; Bordiga, S.; Zecchina, A. *J. Am. Chem. Soc.* **2008**, *130*, 8386.

(36) Caskey, S. R.; Wong-Foy, A. G.; Matzger, A. J. *J. Am. Chem. Soc.* **2008**, *130*, 10870.

(37) Zhou, W.; Wu, H.; Yildirim, T. *J. Am. Chem. Soc.* **2008**, *130*, 15268.

(38) Bhattacharjee, S.; Choi, J. S.; Yang, S. T.; Choi, S. B.; Kim, J.; Ahn, W. S. *J. Nanosci. Nanotechnol.* **2010**, *10*, 135.

(39) Dietzel, P. D. C.; Morita, Y.; Blom, R.; Fjellvåg, H. *Angew. Chem. Int. Ed.* **2005**, *44*, 6354.

(40) Dietzel, P. D. C.; Panella, B.; Hirscher, M.; Blom, R.; Fjellvåg, H. *Chem. Commun.* **2006**, 959.

(41) FitzGerald, S. A.; Burkholder, B.; Friedman, M.; Hopkins, J. B.; Pierce, C. J.; Schloss, J. M.; Thompson, B.; Rowsell, J. L. C. *J. Am. Chem. Soc.* **2011**, *133*, 20310.

(42) Dietzel, P. D. C.; Besikiotis, V.; Blom, R. *J. Mater. Chem.* **2009**, *19*, 7362.

(43) Britt, D.; Furukawa, H.; Wang, B.; Glover, T. G.; Yaghi, O. M. *Proc. Natl. Acad. Sci. U.S.A.* **2009**, *106*, 20637.

(44) Valenzano, L.; Civalleri, B.; Chavan, S.; Palomino, G. T.; Arean, C.; Bordiga, S. *J. Phys. Chem. C* **2010**, *114*, 11185.

(45) Bloch, E. D.; Murray, L. J.; Queen, W. L.; Chavan, S.; Maximoff, S. N.; Bigi, J. P.; Krishna, R.; Peterson, V. K.; Grandjean, F.; Long, G. J.; Smit, B.; Bordiga, S.; Brown, C. M.; Long, J. R. *J. Am. Chem. Soc.* **2011**, *133*, 14814.

(46) Bloch, E. D.; Queen, W. L.; Krishna, R.; Zadrozny, J. M.; Brown, C. M.; Long, J. R. *Science* **2012**, *335*, 1606.

(47) Kittel, C. *Thermal Physics*; John Wiley & Sons, Inc.: New York, 1969.

(48) Langmuir, I. *J. Am. Chem. Soc.* **1918**, *40*, 1361.

(49) FitzGerald, S. A.; Hopkins, J.; Burkholder, B.; Friedman, M.; Rowsell, J. L. C. *Phys. Rev. B* **2010**, *81*, 104305.

(50) FitzGerald, S. A.; Allen, K.; Landerman, P.; Hopkins, J.; Matters, J.; Myers, R.; Rowsell, J. L. C. *Phys. Rev. B* **2008**, *77*, 224301.

(51) FitzGerald, S. A.; Churchill, H. O. H.; Korngut, P. M.; Simmons, C. B.; Strangas, Y. E. *Rev. Sci. Instrum.* **2006**, *77*, 093110.

(52) Leachman, J. W.; Jacobsen, R. T.; Penoncello, S. G.; Lemmon, E. W. *J. Phys. Chem. Ref. Data* **2009**, *38*, 721.

(53) Queen, W. L.; Bloch, E. D.; Brown, C. M.; Hudson, M. R.; Mason, J. A.; Murray, L. J.; Ramirez-Cuesta, A. J.; Peterson, V. K.; Long, J. R. *Dalton Trans.* **2012**, *41*, 4180.

(54) Sumida, K.; Brown, C. M.; Herm, Z. R.; Chavan, S.; Bordiga, S.; Long, J. R. *Chem. Commun.* **2011**, *47*, 1157.

(55) Mason, J. A.; Sumida, K.; Herm, Z. R.; Krishna, R.; Long, J. R. *Energy Environ. Sci.* **2011**, *4*, 3030.

(56) Kong, L. Z.; Román-Pérez, G.; Soler, J. M.; Langreth, D. C. *Phys. Rev. Lett.* **2009**, *103*, 96103.

(57) Czepirski, L.; Jagiello, J. *Chem. Eng. Sci.* **1989**, *44*, 797.

(58) Dietzel, P. D. C.; Georgiev, P. A.; Eckert, J.; Blom, R.; Strassle, T.; Unruh, T. *Chem. Commun.* **2010**, *46*, 4962.

(59) FitzGerald, S. A.; Yildirim, T.; Santodonato, L. J.; Neumann, D. A.; Copley, J. R. D.; Rush, J. J.; Trouw, F. *Phys. Rev. B* **1999**, *60*, 6439.

(60) Myers, A. L.; Prausnitz, J. M. *AIChE* **1965**, *11*, 121.

(61) Tanaka, H.; Noguchi, D.; Yuzawa, A.; Kodaira, T.; Kanoh, H.; Kaneko, K. *J. Low Temp. Phys.* **2009**, *157*, 352.

(62) Cessford, N. F.; Seaton, N. A.; Düren, T. *Ind. Eng. Chem. Res.* **2012**, *51*, 4911.

(63) Li, H.; Eddaoudi, M.; O'Keeffe, M.; Yaghi, O. M. *Nature* **1999**, *402*, 276.

(64) Chui, S. S. Y.; Lo, S. M. F.; Charmant, J. P. H.; Orpen, A. G.; Williams, I. D. *Science* **1999**, *283*, 1148.

(65) Niimura, S.; Fujimori, T.; Minami, D.; Hattori, Y.; Abrams, L.; Corbin, D.; Hata, K.; Kaneko, K. *J. Am. Chem. Soc.* **2012**, *134*, 18483.

9464

dx.doi.org/10.1021/ja402103u | *J. Am. Chem. Soc.* 2013, 135, 9458−9464